J Solid State Electrochem (2011) 15:2419–2425
DOI 10.1007/s10008-011-1442-4

ORIGINAL PAPER

Formation of gold-capped silicon nanocolumns on silicon substrate

K. Leinartas · P. Miečinskas · A. Selskis · V. Janušonienė · A. Galdikas · J. Ulbikas · A. Šetkus · R. Kaliasas · E. Juzeliunas

Received: 18 March 2011 / Revised: 30 May 2011 / Accepted: 31 May 2011 / Published online: 11 June 2011
© Springer-Verlag 2011

Abstract Gold-capped silicon nanocolumns regularly distributed over silicon substrate were obtained. The columns length was roughly 100 nm; their deviation from perpendicular axis was less than 2°. The diameter of the columns was of the order of 10 nm or below of that. The proposed procedure of nanostructuring included the following main steps: deposition of aluminum thin layer (100–500 nm) by magnetron sputtering on (100) oriented Si wafers; formation of porous self-ordered alumina structures by electrochemical anodizing of the Al film in oxalic acid; electroless inversion of Au in alumina pores; and reactive ion etching. The obtained Si–Au structures are of importance as the platforms for biosensing applications, while the gold-free structures are of interest in photovoltaics.

This paper is dedicated to the 65th birthday of Professor G. Inzelt.

K. Leinartas · P. Miečinskas · A. Selskis · E. Juzeliunas (✉)
Center for Physical Sciences and Technology,
Institute of Chemistry,
A. Goštauto 9,
Vilnius 01108, Lithuania
e-mail: ejuzel@ktl.mii.lt

V. Janušonienė · A. Galdikas · J. Ulbikas
Applied Research Institute for Prospective Technologies,
Saulėtekio 15,
Vilnius 10224, Lithuania

A. Šetkus
Center for Physical Sciences and Technology,
Semiconductors Physics Institute,
A. Goštauto 11,
Vilnius 01108, Lithuania

R. Kaliasas
Center of Mechatronics,
S. Daukanto 12,
Panevėžys 35212, Lithuania

Keywords Silicon · Gold · Alumina · Nanopores · Nanocolumns

Introduction

Silicon surface structuring on nano–microscale is of great interest in many multidisciplinary fields such as optoelectronics [1, 2], photovoltaics [3, 4], chemical and biological sensors [3, 5–11], and in vivo biomedical applications [7, 8].

Silicon–gold systems attracted recently substantial attention as promising platforms for chemical and biological label-free sensing. Advantages of gold, as a material, for biosensing applications include biocompatibility and chemical affinity with thiol group to immobilize DNA [12]. Highly selective and precise protein pattering was achieved using microscale gold-patterned silicon substrates [13]. Bovine serum albumin and fibronectin were attached to the gold regions, while this was not a case for immunoglobulin.

It has been shown that the gold nanoparticles, when compared to a bulk material, have increased target binding constant, high sensibility, superior immobilization rates, and enhanced hybridization efficiency [14–18].

Silicon is attractive as a biosensing platform, first of all, due to a possibility of on-chip integration with semiconductor technologies. Another important feature is possibility to obtain large surface-to-volume ratio by electrochemical production of porous silicon and nanoformations [1–3, 18]. Silicon surface can be easily chemically functionalized via the oxide- or the hydrogen-terminated surface.

Silicon nanowires (SiNWs) embedded with gold nanoparticles (GN) are promising platforms for biomolecular sensing. The SiNW–GN sensor was applied for glutathione detection in a solution using cyclic voltammetry [17]. Probe nucleotides were immobilized onto SiNW–GN, and their

hybridization with breast cancer DNA was studied [18]. The system SiNW–GN was used also for detection of bovine serum albumin [19]. The sensor performed well due to large surface area and high electrical conductivity.

Other surface structures such as porous, amorphous, or nanocrystalline ones have been functionalized with GN as well [20, 21]. Jiao et al. prepared a dual-mode sensing platform from porous silicon and colloidal GN, which enabled to study both molecular binding and identification of benzenethiol via measurements of reflectance and SERS [20]. Martins et al. reported an amorphous/nanocrystalline Si with oligonucleotide-derivatized GN for the identification of nucleic acid sequences [21].

Furthermore, silicon-pillared architectures are important as an alternative to a planar design of solar cells. Silicon nano–microrods make it possible orthogonalization of the directions of light absorption and charge-carrier collection. In such architectures, light is absorbed along the axial dimension of the rod, while the charge carrier diffuses much shorter distances radially to a *p–n* junction [22, 23]. The concept opens the route for cheaper solar cells through application of less pure silicon.

Large-scale ordered Si nanowire arrays are usually grown by chemical vapor deposition [24]. The process "vapor–liquid–solid" involves Au, Ag clusters, which are deposited on silicon substrates by vacuum evaporation or electroless deposition in solutions. Formation of single crystalline Si nanowires was also proposed using self-assembly of Ag dendrites on silicon [25]. Si nanowires are formed by electrochemical substrate etching in a solution containing $AgNO_3$ and hydrofluoric acid. Silicon nanowires of 10–30 μm in length and 30–300 nm in diameter were formed by this method. A nanofabrication process via self-assembly of polystyrene spheres on <100> Si plane using reactive ion etching has been proposed [26]. Large-scale and highly ordered arrays of Si nanowires of 6.6 to 8.5 μm in length and 220 to 280 nm in diameter have been obtained.

A perspective way for Si surface nanostructuring is application of porous alumina as an intermediate template for the surface pattering. Electrochemical self-assembly of pores in the aluminum oxide formed by aluminum anodizing has been widely studied [27–46]. Regularly distributed pores develop during the anodizing at the oxide/electrolyte interface. The matrix consists of densely packed hexagonal columnar cells with cylindrical pores in the center. The pore size and the interpore distance range from a few to hundreds of nanometers depending upon the voltage, the electrolyte concentration and the temperature applied.

The majority of the porous alumina studies deals with bulk aluminum substrates. Significantly less is known, however, about porosity formation when anodizing thin aluminum films. The templates formed of thin alumina layers are of increasing interest due to their potential applications in nanotechnologies. Surely, when compared to bulk substrates, experimentation with thin layers requires more precise and strict procedures, and the influence of substrate on template properties is much more pronounced.

There is great research interest and practical demand in new means of preparation of Si–Au and Si nanocolumnar architectures. Here, we report a formation of gold-capped and gold-free silicon nanocolumnar structures, which were obtained via formation of a nanoporous alumina film template on silicon substrate and subsequent electroless gold inversion, reactive ion etching, and acid treatment.

Experimental

Aluminum films of 100–500 nm thickness were deposited on silicon using magnetron-sputtering device "UNIVEX 350" (from Leybold, Germany). P-type silicon (100) wafers of 20 mm in diameter and resistivity of 10–20 Ωcm were used as the substrates. The sputtering device was composed of three confocal magnetrons "ST-20" (AJA International, USA) with possibility to operate in direct current (DC) or radio frequency (RF) modes. Targets were prepared from aluminum (99.999 from Alfa Aesar GmbH, Germany). The device chamber was evacuated down to $(1.2–1.6)\times 10^{-6}$ mbar and filled with argon. Prior to sputtering, the Si substrate was cleaned by Ar^+ ions in RF mode. The RF plasma discharge was maintained at a pressure of 6.5×10^{-3} mbar and 16 W of effective power for 5 min. Sputtering of the target was performed in DC mode. The working gas pressure was maintained at $\sim 1.3\times 10^{-3}$ mbar, and sputtering power was ~270 W.

The Al film anodizing was carried out in 0.3 M oxalic acid (pure p. a. CHEMPUR, Poland) at a temperature of 20 °C using an Agilent 6038 power supply source (USA). The rest of the aluminum barrier layer at the bottom of pores was removed by chemical etching in 5 wt.% orthophosphoric acid at 30 °C.

Au nanocolumns were inverted into the pores of alumina from the electrolyte 0.0002 M $AuCl_3$+0.8 M NH_4F. Solution pH was adjusted to 1.5–2.0 using hydrochloric acid. The rate of Au deposition was about 24 nm/min. Residues of aluminum oxide layer were dissolved in $K_2Cr_2O_7$ solution.

Scanning electron microscope (SEM) EVO-50EP (Carl Zeiss SMT AG, Germany) with microprobe analyzer was used to study composition of the sputtered coatings as well as the surface topography. Alumina layers with pores dimensions of the order of 10 nm were studied by a field emission SEM ("RAITH-e-LiNE" from Raith GmbH, Germany).

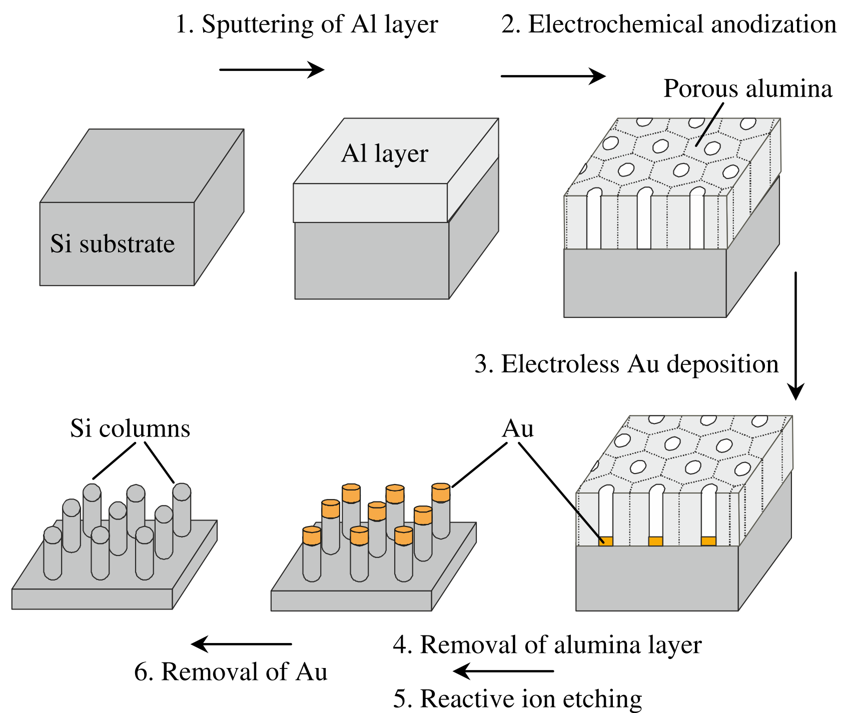

Fig. 1 Schematic diagram of fabrication of nanocolumnar structures via aluminum sputtering, electrochemical anodizing, electroless Au deposition within the pores, reactive ion etching, and gold dissolution

The "Advanced Vacuum Vision 320" system with 13.56 MHz radio frequency integrated with "Raith-e-Line" SEM was used for reactive ion etching (RIE). The modified parallel plate reactor with 13.56 MHz radio frequency was used. The etching conditions were empirically determined to ensure preferential sputtering of unmasked Si. An anisotropic etching process using CF_4 gas was used for Si etching. The procedure was performed at the gas flow rate of 3 to 30 sccm (standard cubic centimeter per minute) and at the pressure of 10 to 20 mTorr ($13–26\times10^{-3}$ mbar). The etching power varied from 25 to 120 W, which corresponded to self-bias on the cathode from −130 to 280 V.

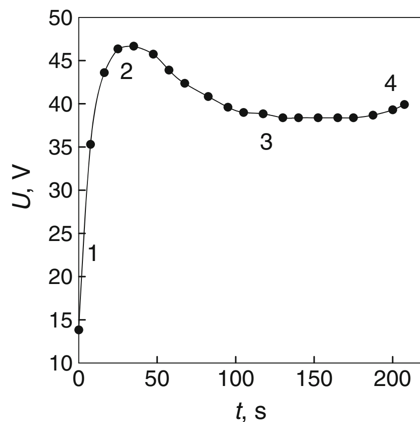

Fig. 2 Voltage vs. time curve of alumina pores formation at $I=4$ mA/cm^2 in 0.3 M oxalic acid. Four distinctive zones are shown on the *curve*, which are explained in the text

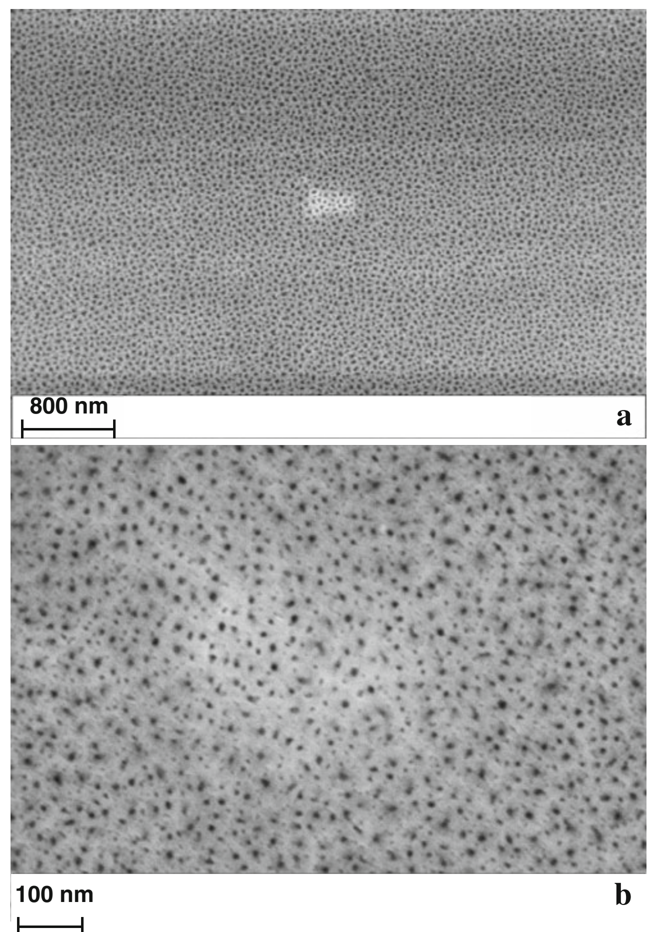

Fig. 3 SEM images of porous alumina formed at anodic bias 20 V **a** and 10 V **b** in 0.3 M oxalic acid

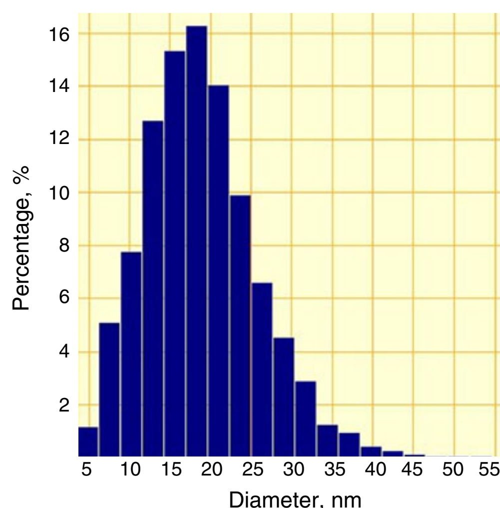

Fig. 4 Histogram of alumina pores formed by anodizing of magnetron-sputtered Al in oxalic acid at E=20 V, I=4 mA/cm^2, t= 240 s and subsequent etching in the 5 wt.% orthophosphorous acid (duration 540 s)

Distribution of nanopores and surface topography was also studied by scanning probe microscopy (SPM) “SPM D3100/ NanoscopeIVa” (VEECO, USA). The surfaces were scanned in noncontact (tapping) and tunneling current modes. The samples were dehumidified for 2−3 h in a special chamber before measurements. The relative humidity less than 5% at 35 °C was maintained in the chamber. Software packages “NanoScope Software 6.13” (VEECO Instr., USA) and “SPIP” (Image Metrology, Denmark) were used for processing of the data. Coating thickness was measured using a profilometer Dektak 6M (VEECO Instr., USA).

Results and discussion

Figure 1 shows a schematic diagram of the proposed fabrication of nanocolumnar structures. The entire process is divided into the following main steps: the thin aluminum film deposition by magnetron sputtering; the pore formation by electrochemical anodizing; the gold inversion within the pores by electroless deposition; the formation of silicon nanocolumns by reactive ion etching and the gold dissolution.

In order to produce nanoporous alumina film template, aluminum films 100 to 500 nm in thickness were deposited on p-type silicon <100> substrate by means of magnetron sputtering. The pores were formed, then, in the coating by its anodizing galvanostatically in 0.3 M oxalic acid.

A typical voltage variation vs. anodizing time curve is shown in Fig. 2. The curve exhibits four distinctive parts. The first one is an ascending part, which is attributable to a barrier formation—a very thin nonporous Al_2O_3 layer on the top of the coating [47]. The pore formation starts already in the first part of the curve (1, Fig. 2), and the process develops in the second part, which is the peak 2 in the figure. The descending part and the more or less stable voltage zone (3) are attributable to depth penetration of the pores [47]. The final part is a current increase (4), which identifies an onset of silicon substrate oxidation. The latter was used in our experiments as a criterion to terminate the anodizing process.

SEM images of the porous alumina formed at E=20 V and E=10 V are given in Fig. 3. Clearly, the nanopores regularly distributed over the surface were obtained, which size is of the order of tens of nanometers.

SPM data in Fig. 4 show that great majority of the pores formed at E=20 V had the size in the range 15 to 25 nm. Reducing of the anodizing bias to E=10 V led to formation of considerably smaller pores (Fig. 5a). In this case, about 30% of the pores were of the size 5 to 10 nm.

The coating sputtered on silicon is getting substantially thinner during the anodizing. Thus, the depth profile in Fig. 6 shows that the initial 100 nm coating reduces in thickness to ca. 20 nm during 120 s of anodizing at 10 V. Surface analysis showed that after the anodizing, some

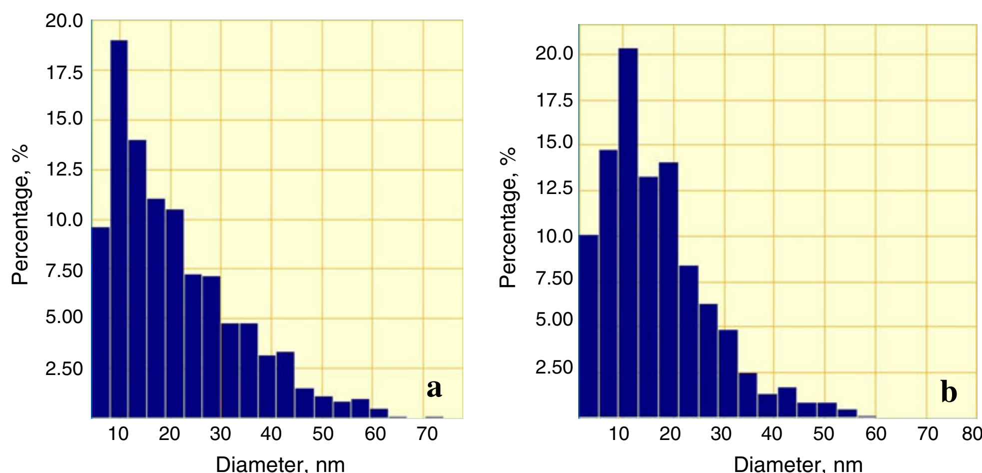

Fig. 5 Histograms of alumina pores. **a** After anodizing in oxalic acid (E=10 V, I=1 mA/ cm^2, t=120 s). **b** After etching of the residues of the barrier layer in 5% orthophosphorous acid (t=360 s)

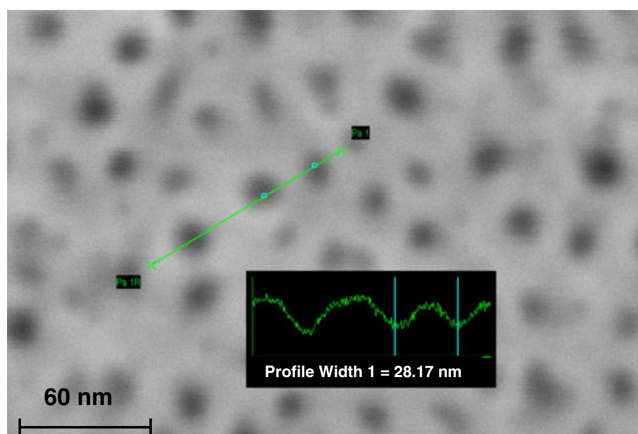

Fig. 6 SEM image and the depth profile of the porous alumina layer on silicon substrate, which was measured *along the line* shown on the SEM image. The treatment conditions are analogous to those given in Fig. 4

residual alumina layer is present on the bottom of the pores. Surface treatment in 5 wt.% orthophosphorous acid was found to be an appropriate procedure to get alumina-free silicon surface in the bottom of the pores and, at the same time, not to substantially increase the pore size.

The profile of the porous alumina surface with the alumina-free silicon surface within the pores is shown in Fig. 6. Obviously, the pore size is of the order of several tens of nanometers, which is comparable to the sizes of untreated pores (Fig. 3). The histogram in Fig. 5b also confirms that the applied acid treatment caused only minor increase in the pore sizes. This is evident from the only slight shift of the histogram maximum when compared to that of acid nontreated sample (Fig. 5a).

Gold particles were inverted into the alumina pores by means of electroless deposition from acid fluoride solution.

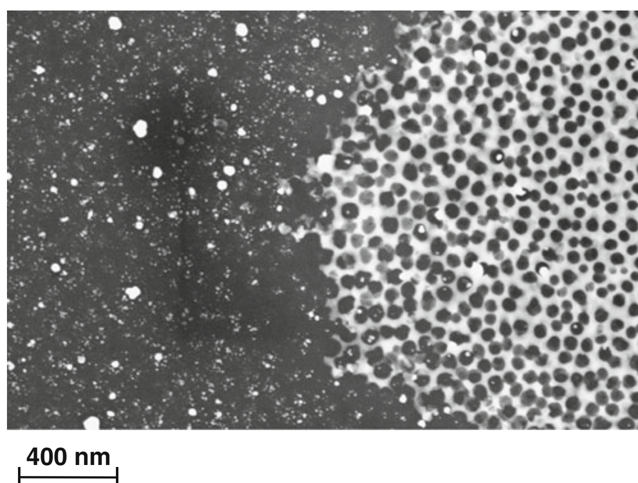

Fig. 7 SEM image of the Si surface with deposited Au particles (*left*). The image shows also the propagation boundary of Au–Si surface. Porous alumina is seen on the *right* part of the image

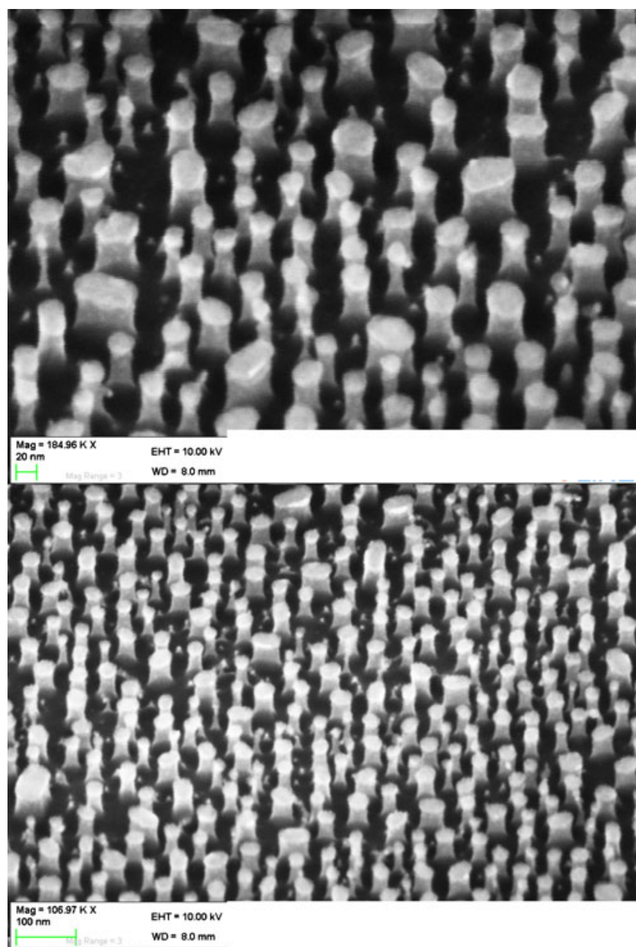

Fig. 8 SEM images of Si surface after 2 min of reactive ion etching

Hydrofluoric acid reacts with silicon (or silica) substrate producing SiF_6^{2-} ions, which further reduce $Au^{3\pm}$ to Au. The electroless deposition takes place in the bottom of the alumina pores only on Si surface because of formation in these sites of the silicon-containing reductor. Some alumina

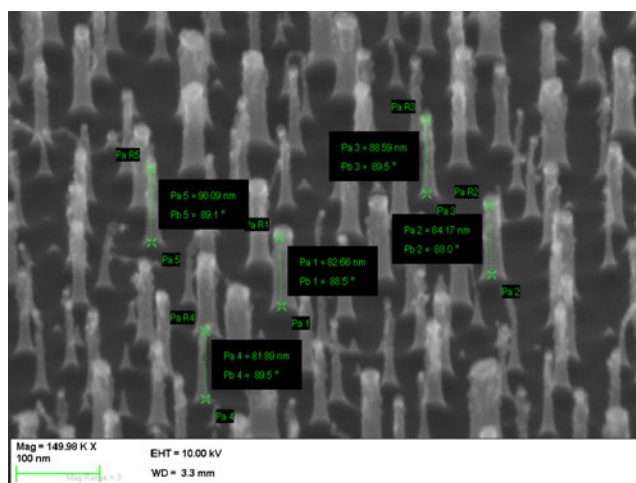

Fig. 9 SEM images of Si surface after 11 min of reactive ion etching

surface dissolution occurs as well; however, aluminum ions do not reduce the gold and, thus, gold deposition occurs within the pores. The reaction mechanism of electroless gold deposition from fluoride solutions was studied by Nagahara et al. [48, 49].

Then, the alumina was dissolved in potassium dichromate. According to our experience, potassium dichromate solution is well suited for "soft" removal of the rest of alumina (sodium or potassium hydroxide solutions are more difficult to remove by washing from the surface by a water stream). Figure 7 shows the silicon surface capped by gold nanoparticles (left) as well as the porous alumina structure with gold particles inside the pores (right). The alumina dissolution boundary is clearly demonstrated as well. The optimum gold deposition time under the applied conditions was found to be around 5 s. A longer treatment led to aggregation of gold particles into larger formations (100 nm, or so), and the size of pores increased due to alumina dissolution. The Au content on the surface was examined by x-ray photoelectron spectroscopy (XPS) measurements. It was found to be ca. 4.5 at.% after 5 s deposition.

The final stage of the surface nanoengineering was the silicon reactive ion etching by CF_4 gas. In such type of plasma, a great variety of ions and radicals is formed: CF_3^+ (~77%) CF_3 (~6.5%) CF, F^+ (~4%), F, etc. Main product of the silicon etching is volatile SiF_4. Some physical surface sputtering takes place simultaneously with the chemical etching as well. Silicon nanocolumns capped with gold particles were formed by this technique. Figures 8 and 9 show typical nanocolumnar structures obtained at different etching conditions and duration. The patterns were formed using CF_4 flow rate of 30 sccm, the pressure of 15 mTorr, and the etching power of 100–150 W. The column high in Fig. 9 is ca. 80 to 90 nm, and the deviations from perpendicular axis are less than 2°. The diameter of the columns is of the order of tens nanometers. Control of etching time allows to easily controlling the shape, the height and the diameter of the columns. It is also obvious that a smaller diameter of Si nanocolumns is obtained at the expense of increase in the intercolumnar distance. The SEM images also show that a significant part of the nanoformations satisfy size requirement for quantum confinement, which is below 10 nm [50]. The gold-free nanocolumnar surface could be easily obtained by sample treatment of the Si–Au samples in "aqua regia".

Conclusions

Gold-capped silicon nanocolumns regularly distributed over silicon substrate were obtained. The columns were around 100 nm in heights with deviations from perpendicular axis less than 2°. Diameter of the columns was of the order of tens nanometers. Significant part of the columns had the diameters below 10 nm, which satisfy size requirement for quantum confinement effect.

The proposed route of the nanostructuring included the following main steps: deposition of aluminum thin layer (100–500 nm) by magnetron sputtering on (100) oriented Si wafers; formation of porous self-ordered alumina structures by anodizing of the Al film in oxalic acid; electroless deposition of Au in alumina pores; treatment in acids; and final treatment of sample surface by reactive ion etching/sputtering.

The obtained Si–Au nanostructures are of importance as the platforms for biochemical sensors. The gold-free structures are of interest in photovoltaic applications.

Acknowledgments The study was supported by the Lithuanian State Science and Studies Foundation (Contract No. AUT-18/2010).

References

1. Collins RT, Fauchet PM, Tischler MA (1997) Phys. Today, January, pp 24–31
2. Canham LT (1990) Appl Phys Lett 57:1046–1048
3. Singh P, Sharma SN, Ravindra NM (2010) JOM 62:15–24
4. Szlufcik J, Agostinelli G, Duerinckx F, Van Kerschaver E, Beaucarne G (2005) Low cost industrial technologies of crystalline silicon solar cells. In: Markvart T, Castauer L (eds) Solar cells: materials, manufacture and operation. Elsevier Ltd., Oxford, pp 91–120
5. Jane A, Dronov R, Hodges A, Voelcker NH (2009) Trends Biotechnol 27:230–239
6. Kilian KA, Böcking T, Gooding JJ (2009) Chem Commun 630–640
7. Anglin EJ, Cheng L, Freeman WR, Sailor MJ (2008) Adv Drug Deliv Rev 60:1266–1277
8. Salonen J, Kaukonen AM, Hirvonen J, Lehto VP (2008) J Pharm Sci 97:632–653
9. Bonanno LM, DeLouise LA (2007) Biosens Bioelectron 23:444–448
10. Lawrie L, Jiao Y, Weiss SM (2010) IEEE Trans Nanotechnol 9 (5):596–602
11. Ozdemir S, Gole JL (2007) Curr Opin Solid State Mater Sci 11:92–100
12. Ohgi T, Sheng HY, Nejoh H (1998) Appl Surf Sci 130:919–924
13. Veiseh M, Zareie MH, Zhang M (2002) Langmuir 18:6671–6678
14. Xu J, Craig SL (2005) J Am Chem Soc 127:13227–13231
15. Lytton-Jean AKR, Mirkin CA (2005) J Am Chem Soc 127:12754–12755
16. Akamatsu K, Kimura M, Shibata Y, Nakano SI, Miyoshi D, Nawafune H, Suginoto N (2006) Nano Lett 6:491–495
17. Yang K, Wang H, Zou K, Zhang X (2006) Nanotechnology 17: S276–S279
18. Ryu SW, Kim CH, Han JW, Kim CJ, Jung C, Park HG, Choi YK (2010) Biosens Bioelectron 25:2182–2185
19. Yan S, He N, Song Y, Zhang Z, Qian J, Xiao Z (2010) J Electroanal Chem 641:136–140
20. Jiao Y, Koktysh DS, Phambu N, Weiss S (2010) Appl Phys Lett 97:153125–3
21. Martins R, Baptista P, Raniero L, Doria G, Silva L, Franco R, Fortunato E (2007) Appl Phys Lett 90:023903–3

22. Kayes BM, Atwater HA, Lewis NS (2005) J Appl Phys 97:114302–114311
23. Maiolo JR III, Atwater HA, Lewis NS (2008) J Phys Chem C 112:6194–6201
24. Tsakalakos L, Balch J, Franheiser J, Korevaar B, Sulima O, Rand J (2007) Appl Phys Lett 91:233117
25. Peng K, Yan Y, Gao S, Zhu J (2003) Adv Funct Mat 13(2):127–132
26. Huang Z, Fang H, Zhu J (2007) Adv Mater 19:744–748
27. Masuda H, Fukuda K (1995) Science 268:1466–1468
28. Masuda H, Hasegwa F, Ono S (1997) J Electrochem Soc 144: L127–L130
29. Ono S, Saito M, Asoh H (2005) Electrochim Acta 51:827–833
30. Chu Z, Wada K, Inoue S, Isogai M, Katsuta K, Yasumuri A (2006) J Electrochem Soc 153:B384–B391
31. Jessensky O, Muller F, Gösele U (1998) J Electrochem Soc 145 (11):3735–3740
32. Jessensky O, Muller F, Gösele U (1998) Appl Phys Lett 72:1173–1175
33. Meng G, Jung YJ, Cao A, Vajtai R, Ajayan PM (2005) PNAS 102 (20):7074–7078
34. Keller F, Hunter MS, Robinson DL (1953) J Electrochem Soc 100:411–419
35. Diggle J, Downie T, Goulding C (1969) Chem Rev 69(3):365–405
36. O'Sullivan J, Wood GC (1970) Proc R Soc Lon A317:511–543
37. Hoar T, Mott N (1959) J Phys Chem Solids 9:97–99
38. Shimuzu K, Kobayashi K, Tompson GE, Wood GC (1992) Phil Mag A 6:643–652
39. Li AP, Muller F, Birner A, Nielsch K, Gösele U (1998) J Appl Phys 84:6023–6026
40. Garcia-Vergara SJ, Iglesias-Rubianes L, Blanco-Pinzon CE, Skeldon P, Thompson GE, Campestrini P (2006) Proc R Soc A 462:2345–2358
41. Masuda H, Satoh M (1996) Jpn J ApplPhys 35:L126–L129
42. Zhu R, Pang YT, Feng YS, Fu GH, Li Y, Zhang LD (2003) Chem Phys Lett 368:696–700
43. Shingubara Sh, Murakami Y, Morimoto K, Takahagi T (2003) Surf Sci 532–535:317–323
44. Nakao M, Oku S, Tamaura T, Yasui K, Masuda H (1999) Jpn J Appl Phys 38:1052–1055
45. Mei X, Blumin M, Kim D, Wu Zh, Ruda H (2003) J Cryst Growth 251:253–257
46. Gao SY, Li HD, Yuan JJ, Li YA, Yang XX, Liu JW (2010) Appl Surf Sci 256:2781–2785
47. Das B (2004) J Electrochem Soc 151(6):D46–D50
48. Nagahara L, Ohmori T, Hashimoto K, Fujishima A (1992) J Electroanal Chem 333:363
49. Nagahara L, Ohmori T, Hashimoto K, Fujishima A (1993) J Vac Sci Technol A11:763
50. Wiggers H, Lorke A (2011) Silicon nanocrystals. In: Sattler K (ed) Handbook of physics. Nanoparticles and quantum dots, CRC Press, Taylor & Francis Group, pp 5–1